Volume 1 | Number 1 | Jan 2013 | Pages 1–100

Journal of
**Materials Chemistry A**

Materials for energy and sustainability
www.rsc.org/materialsA

Li⁺

e⁻

Li⁺

e⁻

Li⁺

Li⁺

ROYAL SOCIETY
OF CHEMISTRY

ROYAL SOCIETY
OF CHEMISTRY

www.rsc.org/materialsA

# Journal Name

## ARTICLE

# Temperature-induced Au nanostructure synthesis in a nonaqueous deep-eutectic solvent for high performance electrocatalysis†

S. Kumar-Krishnan,[a] E. Prokhorov,[a] O. Arias de Fuentes,[a,b] M. Ramírez,[c] N. Bogdanchikova,[d] I.C. Sanchez,[e] J.D. Mota-Morales[f] * and G. Luna-Bárcenas[a]*

Structure-controlled synthesis of gold nanostructures (AuNSs) induced by temperature in a nonaqueous urea-choline chloride deep eutectic solvent (DES) is reported. Modulation of nanostructures with well-defined structures and shapes are obtained by simply varying reaction temperature. The supramolecular soft template provided by DES structure and its viscosity at different temperatures drives directed growing of crystalline gold and self-assembly producing star-shaped AuNSs. Additionally, the effect of AuNSs shape and surface area on their catalytic activity towards the reduction of hydrogen peroxide ($H_2O_2$) has been tested. With the advantage of their high surface area and presence of high-index facets in the edge of the star arms, the star-shaped nanostructures showed superior electrocatalytic activity than other morphologies. The use of DES as green chemistry platform to shape-control Au nanostructures with high catalytic properties may offer new avenues for fuel cell and biosensor applications.

## Introduction

Controlling the shape of nanomaterials is of paramount importance in the rapidly growing field of nanotechnology and materials science.[1] Noble metal nanoparticles, particularly gold nanoparticles, have gained significant interest due to their unusual physicochemical properties and wide range of potential applications in different fields.[2] The properties of nanoparticles strongly depend on their size, shape, crystallinity and structure, which determine their specific applications.[3] In particular, metal nanoparticles with high-index facets surfaces exhibit fascinating surface-enhanced and catalytic properties compared to spherical ones.[4] It was recently shown that Au nanoparticles with high-index facets exhibits facet-dependent catalytic activities.[5] Therefore, special attention has been focused to synthesizing gold nanostructures with controlled shape enclosed with high-index facets. Additionally, star-shaped gold nanostructures are being developed for promising

applications in sensing, catalysis, SERS and highly efficient photothermal cancer therapy.[6]

Within the framework of green chemistry, deep-eutectic solvents (DESs) emerged as a new type of green solvents that represent an inexpensive alternative to ionic liquids.[7] DESs are generally obtained by complexation of ammonium salts with hydrogen bond donors, to form a eutectic mixture with melting points below their individual constituents.[8] DESs have been recently used for a wide range of applications in polymer science, supercapacitors, biocatalysis, energy storage, extraction of natural compounds, biomedicine and controlled release of drugs.[9] Distinctive features of DES such as extended hydrogen bond structure in liquid state, ionic character, negligible volatility, bio-degradability, non-toxicity and low cost make DESs particularly desirable as nonaqueous green media for the shape-controlled synthesis of nanostructures and functional materials.[10] Furthermore, DESs have demonstrated to play multiple roles in nucleation, growth, self-assembly and formation of well-defined frameworks of metallic nanoparticles.[8-9, 10]

Since the work of Sun and co-workers,[11] only a few DES-assisted synthesis of metallic nanoparticles with controlled shapes have been reported.[4c, 4d, 12] For instance, Wei et al. recently explored the formation of nanoflowers and triambic icosahedral platinum nanocrystals enclosed by [771] high index facets using an electrochemical method.[4c, 4d, 12c] They found that such high index-facets exhibited enhanced catalytic activity. Other studies also demonstrated shape-controlled syntheses of Au nanostructures such as self-assembled spherical nanoparticles, stars, nanowire networks and microstructures mediated by DES.[12a, 12d-f] DES properties, such

a. Cinvestav Queretaro, Querétaro QRO, 76230, México. E-mail: gluna@qro.cinvestav.mx
b. Instituto de Ciencia y Tecnología de Materiales, Universidad de La Habana, 10400, Cuba.
c. Centro de investigaciones en Ciencias de la Tierra y Materiales, Universidad Autónoma del Estado Hidalgo, Pachuca, HGO 42184, México.
d. Department of Chemical Engineering, The University of Texas at Austin, Austin, TX 78712, USA.
e. Centro de Nanociencias y Nanotecnología-UNAM, Ensenada BC, 22860, México.
f. Cátedras Conacyt at Centro de Nanociencias y Nanotecnología-UNAM, Ensenada BC, 22860, México. E-mail: mota_josue@hotmail.com; jmota@cnyn.unam.mx
† Electronic Supplementary Information (ESI) available: TEM, UV-Vis and EDS analysis of gold nanostructures, their size distribution, and details about the cyclic voltammograms. See DOI: 10.1039/x0xx00000x

as viscosity, density and surface tension strongly depend upon the temperature and water content.[13] However, to the best of our knowledge, no reports have elucidated the effect of temperature on the shape of gold nanostructures synthesized in DESs.

Herein, we report a strategy to thermally-induce different structures and morphologies of metallic gold nanostructures (AuNSs) in a nonaqueous DES. Our synthesis method does not involve the use of seeds, surfactants or stabilizers other than the DES itself. The final shape and size of AuNSs can be simply tuned by varying the reaction temperature. The resultant AuNSs were characterized by UV-Vis, SEM, TEM, XRD and XPS analyses. Furthermore, the catalytic performance of as-prepared AuNSs was studied by the electrocatalytic reduction of $H_2O_2$ using cyclic voltammetry (CV) analysis.

Our research focuses on the effect of temperature during the reduction of a gold salt in DES. In contrast, previous reports of DES-assisted synthesis of Au nanostructures studied their morphology depending upon the concentration of ascorbate ions (reducing species) and water content. For instance, Liao et al.[11] reported star-shaped gold nanoparticles synthesized by chemical reduction in DES at room temperature. They found that by adding small amounts of water to the DES medium facilitated the formation of star-shaped AuNPs; however, reaction times ranged from several hours to up to a week, at room temperature. Additionally, Stassi et al.[12b] studied the effect of ascorbate ions concentration and water content on Au nanoparticle's final morphology. It is noteworthy that at certain water concentration in DES, poor control over the size and shape of resulting gold nanostructures was observed. Our work demonstrates that well-defined and homogeneous multibranched growth of AuNS with high yields is feasible by performing gold chemical reduction in DES as a function of temperature.

## Experimental

### Materials

Gold (III) chloride hydrate ($HAuCl_4.4H_2O$), L-ascorbic acid (≥99%), urea 99%, and choline chloride (ChCl) 98% were purchased from Sigma Aldrich. Hydrogen peroxide $H_2O_2$ (30 wt.%) was purchased from Merk. All reagents were analytical grade and used as received. Ultrapure water (18 mΩ·cm$^{-1}$) was used for all experiments. All glassware was cleaned with deionized water and air-dried before use in experiments.

### Deep eutectic solvent (DES) preparation

DES was prepared according to well-established procedure previously documented. Briefly, deep-eutectic mixtures counterparts, choline chloride (ChCl) and urea were mixed together in a molar ratio of 1:2 respectively and heating at 80 °C until a homogeneous liquid was obtained. After that, it was cooled to room temperature in a closed vial and then used for further synthesis work.

### DES mediated synthesis of gold nanostructures

In a typical synthesis procedure, four sets of $HAuCl_4.4H_2O$ (10 mg) precursor and L-ascorbic acid (25 mg) were added to 10 mL of freshly prepared DES solvent separately and stirred at different temperature (30 °C, 60 °C, 90 °C and 120 °C) until they completely dissolved. Four different DES mixtures containing $HAuCl_4.4H_2O$ were heated at different temperatures (30 °C, 60 °C, 90 °C and 120 °C) for 30 minutes. Then, DES containing L-ascorbic acid solution was added slowly to the respectively $HAuCl_4.4H_2O$ solution under magnetic stirring. Every final solution mixture was closed tightly and stirred for 1 h without any exposure to light. The final reaction mixtures turned from yellow to dark purple, suggesting the formation of metallic gold of nanometric size. The resulting solutions were centrifuged by adding equal amount of water at 6000 rpm five times to obtain the AuNSs without DES. Finally, the AuNSs were re-dispersed in water for further use.

### Preparation of working electrodes

The working electrodes were homemade glassy carbon electrodes (GCE) carefully polished until obtaining a mirror surface so they were clean and had a reversible electron transfer. Cleaned GC electrodes were dried with nitrogen stream. After that, as prepared AuNSs at different temperatures were dispersed in Milli-Q water and sonicated for 15 minutes to obtain homogeneously dispersed AuNS solution (1.5 mg mL$^{-1}$). Then the homogeneously dispersed AuNS (30 µl) was drop casted onto the surface of the pretreated GCE and left to dry at room temperature to obtain AuNS-modified GCE.

### Electrochemical measurements

All electrochemical experiments were performed using a standard three-electrode electrochemical analyzer (VoltaLab 40 PGZ 301). Platinum wire was used as the auxiliary electrode while a saturated calomel electrode (SCE) as the reference one. The catalytic performance of Au nanostructures modified GCE toward the $H_2O_2$ reduction were carried out using cyclic voltammetry (CVs) measurement. The CVs were recorded in 0.1 M PBS (pH 7.4) in $N_2$-saturated in the absence and presence of different concentration of $H_2O_2$ (1-5 mM). Chronoamperometry (CA) experiments on Au nanostructures prepared at different temperatures were performed for 60 seconds at 0.65 V. The results for 3 mM $H_2O_2$ were taken for the comparison of different Au nanostructures on modified electrodes.

### Materials characterization

UV-Vis absorption spectra were recorded in the range of 300-1100 nm using UV-Vis spectrophotometer (Agilent 8453). The SEM images were obtained from JEOL-JSM7401F field emission scanning electron microscope. The average size-distribution histograms of the SEM images were obtained using ImageJ software. Transmission electron microscope (TEM) images were obtained by JEOL (JEM-1010) operated at 80 kV. Scanning transmission electron microscopy (HAADF-STEM) analyses were obtained using JEM ARM 200F equipment operating at accelerating voltage of 200 kV. X-ray diffraction spectra were acquired using a Rigaku diffractometer ULTIMA IV, equipped with the CuKα radiation (λ=1.5406 Å). X-ray photoelectron spectroscopy (XPS) was carried out using XPS110 instrument from ThermoElectron (East Grinstead, UK) with monochromatic Al-kα. The calibration of the binding

energy of the spectra was performed with the C1s peak of the carbon due to atmospheric contamination, 284.8 eV. The XPS peaks were fitting with the software AAnalyzer® v1.1.Electrochemical measurements were performed on an electrochemical workstation (VoltaLab 40 PGZ 301).

## Results and discussion

In DES formulations, absence of water potentially allows a wide range of synthetic conditions (e.g. temperature and pressure) previously inaccessible due to water evaporation.[9c] For many applications previously described, nonaqueous conditions allows speeding up reaction without sacrificing control over the morphology of AuNS.

To determine the effect of temperature in the shape of gold nanostructures, a series of experiments were performed varying the reaction temperature. The shape of the resultant nanostructure was determined using scanning electron microscopy (SEM) and transmission electron microscopy (TEM) analysis. It can be seen from SEM images (Figure 1) that the growing of AuNS into different shapes depends upon the reaction temperature. At low temperature (e.g. 30 °C), formation of flowerlike structure was observed (Figure 1a,b). When increasing the reaction temperature at 60 °C, a well-defined growth of urchin-like nanostructures was achieved (Figure 1c,d) with size ranging from 300 to 550 nm. A further temperature increase to 90 °C produced the formation of star-shaped structure (Figure 1e,f). Finally, agglomerated branched AuNSs were formed at the higher temperature of 120 °C (TEM images are shown in ESI Figure S1). It is noteworthy that the time to complete the reduction of gold salt (monitored by UV-Vis spectroscopy) significantly decreases with increasing the reaction temperature. This decrement in the reaction time is accompanied by a reduction in the core size of the AuNSs.

The formation of AuNSs was evidenced by UV-vis, energy dispersive X-ray spectroscopy (EDS) and X-ray photoelectron spectroscopy (XPS) measurements. The typical UV-Vis spectra of as-prepared Au nanostructures exhibit the absorption peak at 556 nm that is characteristic of the absorption profile of gold nanoparticles.[12a] Also, the surface plasmon resonance (SPR) peak of the AuNSs prepared at 60 °C shifts to 525 nm compared to the one at 556 nm of those formed at 30 °C; this shifting indicates the formation of lower size particles. (ESI. Figure S2). EDS also indicates that the AuNSs were composed entirely of gold. Nevertheless, it is important to mention that traces of Cl$^-$ were observed, which comes from surface stabilization of DES provided by the choline chloride (ESI. Figure S3). These results suggest deeper implications on the growing mechanism of AuNS, which will be discussed below. The XPS spectra shows that the Au 4f core levels at binding energy (BE) values of 82.5 and 85.15 eV correspond to 4f7/2 and 4f5/2 core levels of Au$^0$ species (Figure 2a).[14] The X-ray powder diffraction (XRD) pattern of as-prepared AuNSs at different temperatures (Figure 2b), showed peaks at 2θ values of 38.0, 44.2, 64.40, 77.7, 81.7 and 98.2 corresponding to (111), (200), (220), (311), (222) and (400) planes of face centered cubic (fcc) structure (JCPDS no.04-0784)

respectively.[15] Interestingly at higher temperature (120 °C) the (400) peak intensity significantly decreased indicating a disordering during the growing of AuNSs at high temperature.
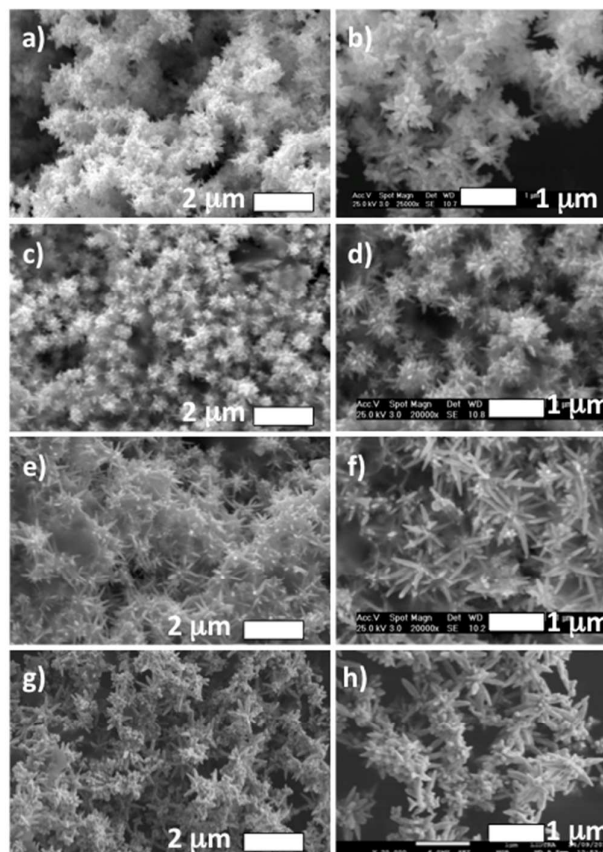


**Figure 1.** Typical FESEM images of the Au nanostructures prepared at different reaction temperature. (a, b) 30 °C (c,d) 60 °C (e, f) 90 °C (g, h) 120 °C.
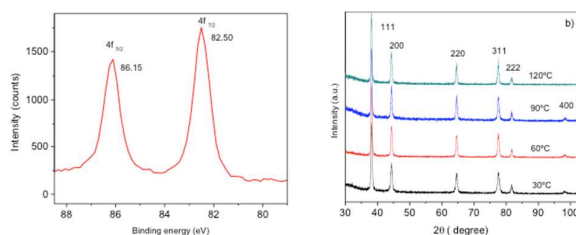


**Figure 2**. a) XPS spectra of Au4f region of as-prepared Au nanostructures b) XRD pattern of the Au nanostructures prepared at different temperatures

To understand the intrinsic crystal structure of the AuNSs, a more detailed investigation was carried out using scanning transmission electron microscopy (STEM) on the sample prepared at 90 °C. Figure 3a shows the representative HAADF-STEM image of AuNSs, which indicates that well-defined star-

shaped AuNSs with sharp edges was formed. Figure 3b shows the HAADF-high resolution STEM (HR-STEM) images of single AuNSs, recorded from the different sections in the sharp edges of the single AuNSs (marked with boxes in Figure 3b).

The five-fold star-shaped NP's (Figure 3) are characterized by two types of tetragonal subunits growing along direction [001].[16] The first corresponds to a combined form {111}/{113}/{331}/{110} of the fcc lattice of Au. In this case, the observed planes by HRTEM are: (111) with a d-spacing of 2.36 Å and (220) –{110} planes– with a d-spacing of 1.44 Å (Figure 3d). In the case of the {110} planes, they do not form apparently facets of the subunit because they are situated parallel to the plane of HRTEM picture, but they are one of the principal planes within the stars since it marks the growing direction of the subunits (Figure 3d). (110) planes appear as the longitudinal section of subunits, whereas (001) planes represent the transversal section. In fact, the zone axis with five-fold symmetry (common to all the subunits and central axis of the twinning superstructure) is clearly located about the direction [110]. On the other hand, the other type of subunit has been reported elsewhere[11, 17] and is constituted by a different combined form: {331}/{110}. It is differentiated from the former by a complete crystallization of a tetragonal sphenoid –{331}– along the direction [001] truncated up-and-down by pinacoid facets {110}. Although in this case, the presence of facets {111} is not delimiting the subunit, estimations of d-spacing would indicate the existence of these planes (Figures 3e). Figures 3e and 3f are effectively clear HRTEM pictures of the diffraction of both planes and facets {331}/{110}. The whole of subunits are grown over the cubic faces {001} with twinned planes about {111}. So, it is hypothesized that the most stable combined form is a cuboctahedron that has growth epitaxially over one face {110} or, in other words, the on-growing planes or growth matrix (planar substrate) of this cuboctahedron are the faces {110}. The pole of this latter plane is coincident with a five-fold axis in the center of the multiple twinning. The former type of subunit (i.e., combined form {111}/{113}/{331}/{110}) appears as a more metastable form than form {331}/{110} in view of the interruption of the growth of sphenoid {331} by the competition with the growth of sphenoid {113}. In the same type of subunit, a face (001) on the final edge (inferior left corner of Figure 3b) develops together with the growth of a small combined form {331}/{110} on another terminal face (001) (superior right corner of Figure 3b). This latter scenario would be interpreted as a secondary binary-twinning with the twinned surface on (001) and, consequently, an additional signal of metastability. Otherwise, differences of intensity of peak (400) with relation to the temperature in GIXD pattern would indicate different steps on facets {331}.

It has been shown that anisotropic growth of AuNSs can be facilitated and directed by specific surfactants or solvents.[18] Conversely several studies demonstrated that the formation of such structures is not related to the specific surfactants or solvents. For instance, derivatives of L-ascorbic acid (reducing agent) play key role in the preferential anisotropic growth of multiple twined crystals with five-fold symmetry or single

crystallinity.[6a, 19] Also, it was reported that oxygen can react with L-ascorbic acid producing hydroxyl radicals, which are responsible for the temperature dependent growth of anisotropic structure.[20] DES exhibits a supramolecular hydrogen-bonding structure, an ionic environment and unusual electrostatic conditions. Those features promote self-assembling and anisotropic growing of nanostructures into a variety of different shapes. Thus DES can act as soft template for the synthesis of well-defined nanostructures, either metallic or metal oxides.[21] It is noteworthy that varying the temperature can significantly modify the physicochemical properties of DES, such as viscosity, density and surface tension.[8-9] Recently, it was reported that DES induce aggregation of Au nanoparticles on the DES through different methods (sputtering and electrochemical).[12a, 12d, 21i] Also the nucleation and aggregation rates in gold nanoparticle synthesis are highly influenced by the specific reducing agents, solvents/stabilizing agents and reaction temperature.[2a]
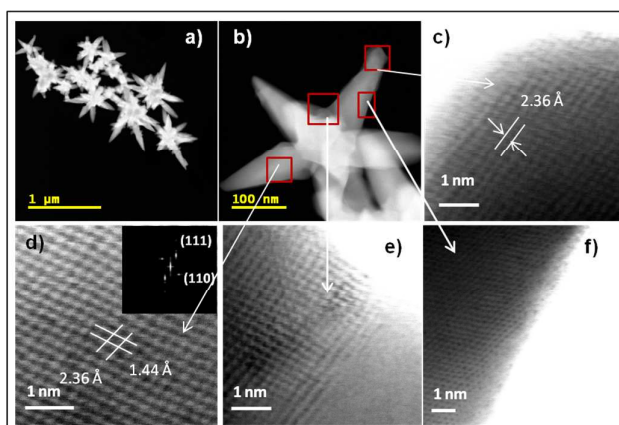


**Figure 3**. a) STEM images of Au nanostructure prepared at 90 °C. b) STEM image of a typical individual Au nanostructure. (c-f) HR-STEM images of sections marked in (b). Inset of d) shows corresponding FFT pattern.

In our study, formation of flowerlike Au nanostructure of ca. 900 nm (Figure 1 a,b) was achieved close to ambient temperature (30 °C). The creation of nucleation sites and subsequent self-assembly and aggregation processes are slow because of poor mass transport that is a direct consequence of the high viscosity of DES. Similarly self-assembly and growth into microstructures have been observed with PbS in DES.[21b] On the other hand, well-defined growth of urchins-like AuNS with lower size has been observed upon increasing the reaction temperature to 60 °C (Figure 1 c,d). At this temperature, L-ascorbic acid oxidation leads to faster nucleation;[12a] also self-assembling and aggregation rates rise yielding a well-defined Au nanourchin shapes. This well-defined growth was promoted by the proper combination of the templating supramolecular structure and viscosity of DES (the viscosity of pure urea-choline chloride DES drops from 1372 mPa·s at 20 °C to 120 mPa·s at 30 °C and to 68.7 mPa·s at 60 °C).[22] Consequently, well-defined urchins shape Au

nanostructures were formed. This phenomenon was evidenced by the following two observations: (1) the significant reduction in the reaction time from 45 min to 15 min (ESI Figure S6) at 90 °C and (2) the size of the nanostructure was reduced while the number of "spikes" in nanostructures increased (Figure 1c,d). The decrease in the reaction time is a consequence of faster reduction of gold salt accompanied by the creation of more nucleation sites, while faster self-assembly and aggregation of small crystals occurs due to the significant drop in DES's viscosity. Interestingly, further increase in the temperature to 90 °C, leads the urchin-like Au nanostructures turning into star-shaped AuNSs, with all other experimental conditions unchanged. Also, the core size was reduced while the length of the arm was increased; this observation may be attributed to the higher reduction and aggregation rates at 90 °C when compared to those at 60 °C (Figure 1e-f and ESI Figure 5). By increasing the temperature (120 °C) formation of network comprising branched AuNSs was observed (Figure 1g-h). This is consistent with the XRD results (Figure 2b), where at 120 °C, the (400) peak disappeared suggesting a disordered preferential growth of AuNSs. Higher temperatures (e.g. 150 °C) and different molar ratio of the DES components (e.g. 1:1) did not showed better results in terms of the presence of high index facets (ESI Figure S7 and S8).

These results demonstrated that the reaction temperature, which in turns affected the reduction rate of gold and DES's viscosity, predominantly controls the evolution shape of different AuNS. In this regard the presence of remaining chloride ions in the surface of some gold structures evidenced by EDS gives clues about the soft templating mechanism of DES. It is plausible that chloride ions act as passivation agent of particular crystal faces directing the preferential growth towards certain crystallographic directions that otherwise are non thermodynamically favorable.[23] At the same time the cation component of DES (cholinium) acts as stabilizer, similarly to cetyltrimethylammonium.[24] Finally, the overall DES as solvent (choline chloride and urea) modulates the mass transport and reactivity of ascorbate ions during reduction of gold cations.[12a]

Numerous studies have been shown that high-facets metal nanostructures exhibit superior catalytic activity due to presence of high-energy surfaces provided by the high density of stepped atoms.[4a, 4d, 12c, 25] For instance, Sun et al. have recently shown that, Pt nanocrystals with high-index facets enclosed by [771], exhibited remarkable enhancement in the electrocatalytic activity toward ethanol oxidation.[4d] Similarly, Liao et al. reported that star-shaped gold nanostructures exhibit excellent electrocatalytic ability for $H_2O_2$ reduction.[11] In the same line, it was reported that Au-Pt and Au-Pd nanometric flowerlike morphologies significantly enhance the electrocatalytic performance.[26] Also, Zhang et al. further evidenced that the catalytic activities of AuNPs are shape and facet-dependent.[5c]

To evaluate the electrocatalytic properties of Au nanostructures, $H_2O_2$ reduction was chosen as probe reaction. Electrochemical studies on samples prepared at various temperatures were performed under the same conditions to

elucidate the effect of different AuNS morphologies. Figure 4a shows the cyclic voltammetry (CV) for the reduction of $H_2O_2$ (3 mM) on the AuNSs modified glassy carbon electrode (GCE) in $N_2$ saturated PBS (pH 7.4) at a scan rate of 50 mV s$^{-1}$. All bare GCE used exhibit similar electrochemical behavior (ESI Figure S9). The electrochemically active surface area (ECSA) was evaluated for the different AuNSs modified GCE. The ECSA for Au nanostars obtained at 90 °C is 0.514 cm$^2$, which is higher than that of other morphologies due to the presence of sharp arms. (ESI Figure S5). The specific reduction current densities ($j_p$) of the AuNSs modified GCE has been normalized based on the ECSA of the respective AuNSs.
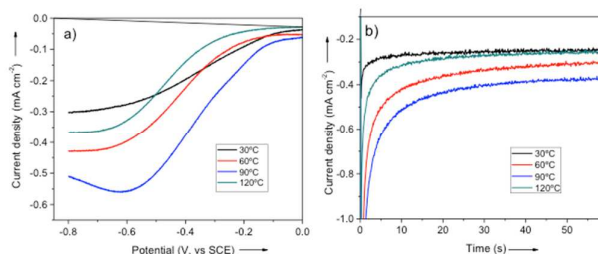


**Figure 4**. a) Comparison of the electrocatalytic activity of Au nanostructures prepared at different temperatures. b) CV curves of electrocatalytic reduction of 3 mM of $H_2O_2$ in 0.1 M PBS (pH 7.4) at a scan rate of 50 mV s$^{-1}$ in nitrogen saturated condition. b) Chronoamperometric curves of $H_2O_2$ (3 mM) reduction at -0.65 V.

Figure 4 shows the presence of reduction peak around -0.65 V that is ascribed to the electrochemical reduction of $H_2O_2$ indicating a good catalytic activity of as-prepared AuNSs. The maximum current densities ($j_p$) values at fixed potential (-0.65 V) obtained with different shapes of Au nanostructure are listed in Table 1. The reduction current varies as a function of the Au nanostructure suggesting that the catalytic activity of as-prepared AuNSs is shape-dependent. Interestingly, there is a significantly higher electrocatalytic reduction current observed for the star-shaped Au nanostructures (90 °C) compared to the flower and urchins shaped Au nanostructure prepared at lower temperature (30 °C and 60 °C), respectively. Moreover, the shifts of the maximum reduction current peaks from -0.65 V to -0.595 V for reduction of $H_2O_2$, also reveals a higher electrocatalytic activity of star-shaped Au nanostructures (Figure 4a).

The chronoamperometry curves at -0.65 V potential recorded for 60 s are shown in Figure 4b and the corresponding steady current density values clearly demonstrate that the star-shaped Au nanostructures (prepared at 90 °C) exhibit significantly higher reduction current density toward $H_2O_2$ over the other shapes (Table 1). In previous reports[6c, 27] using Au stars shaped and Ag-Au bimetallic nanostructures with comparable shape and size, the maximum reduction current was 45 and 57 µA cm$^{-2}$ for 3 mM of $H_2O_2$, respectively.

It is noteworthy that these results are significantly lower than the star-shape AuNSs reduction activities. Beside their method of preparation involved aqueous solutions of surfactants and directing agents. The results disclosed here are also

comparable with the catalytic activity of symmetric 5-fold gold nanostars synthesized at room temperature in DES,[11] with the difference that our approach renders gold nanostructures much faster using mild and anhydrous conditions without sacrificing performance.

**Table 1**. Comparison of the maximum current densities ($j_p$) at fixed potential (-0.65 V) and steady current densities ($j_{60s}$) for Au nanostructures prepared at various temperatures.

| Reaction Temperature (°C) | Observed morphology of AuNSs | $j_p$ (mA cm$^{-2}$) | $j_{60s}$ (mA cm$^{-2}$) |
|---|---|---|---|
| 30 | flower | -0.286 | -0.252 |
| 60 | urchins | -0.422 | -0.338 |
| 90 | star | -0.559 | -0.428 |
| 120 | branched structure | -0.359 | -0.278 |

The higher electrocatalytic activity of Au star-shaped nanostructures can be ascribed to: (1) the high index-facets surfaces, twinning interfaces and high density of stepped atoms in the surfaces of the arm serve as active sites for chemical reduction.[4a, 25, 28] (2) the presence of significantly higher specific surface area of the large star-shaped AuNS shows a large exposed portion which contributes to the significantly higher catalytic activity. The observed results are also consistent with the pentacle shaped Au-Cu bimetallic nanocrystals exhibited higher catalytic activity than citrate capped small spherical nanoparticles and nanorod network.[29]

## Conclusions

The effect of temperature in the controlled-shape synthesis of gold nanostructures in anhydrous conditions has been studied. Reaction temperature, which in turns affects the viscosity of DES, plays a key role in the growing mechanism of Au nanostructures into different shapes exhibiting high-index facets and stepped edges. The formation of such high-index facets structures obeys a self-assembly process directed by the DES via the supramolecular templating that mediate the growing of gold crystalline phases. Cyclic voltamperometry results demonstrated that the as-prepared Au nanostars exhibits remarkable electrocatalytic activity towards $H_2O_2$ reduction compared to other shapes synthesized with different temperatures. The present study provides a green platform from which further exploration of shape-controlled synthesis of other metal nanoparticles with well-defined nanostructure can be exploited for catalysis. DES-assisted synthesis of Au nanostructures may offer potential applications in electrocatalysis, electrochemical biosensors and fuel cells.

## Notes and references

1  B. Lim, Y. Xia, *Angewandte Chemie International Edition* **2011**, 50, 76-85.
2  aM. Grzelczak, J. Perez-Juste, P. Mulvaney, L. M. Liz-Marzan, *Chemical Society Reviews* **2008**, *37*, 1783-1791; bN. Li, P. Zhao, D. Astruc, *Angewandte Chemie International Edition* **2014**, *53*, 1756-1789.
3  R. Gramage-Doria, J. N. H. Reek, *Angewandte Chemie International Edition* **2013**, *52*, 13146-13148.
4  aN. Tian, Z.-Y. Zhou, S.-G. Sun, Y. Ding, Z. L. Wang, *Science* **2007**, *316*, 732-735; bZ.-Y. Jiang, Q. Kuang, Z.-X. Xie, L.-S. Zheng, *Advanced Functional Materials* **2010**, *20*, 3634-3645; cL. Wei, Y.-J. Fan, N. Tian, Z.-Y. Zhou, X.-Q. Zhao, B.-W. Mao, S.-G. Sun, *The Journal of Physical Chemistry C* **2011**, *116*, 2040-2044; dL. Wei, Z.-Y. Zhou, S.-P. Chen, C.-D. Xu, D. Su, M. E. Schuster, S.-G. Sun, *Chemical Communications* **2013**, *49*, 11152-11154.
5  aS. Yang, H. Lee, *ACS Catalysis* **2013**, *3*, 437-443; bM. J. Kale, T. Avanesian, P. Christopher, *ACS Catalysis* **2014**, *4*, 116-128; cQ. Zhang, H. Wang, *ACS Catalysis* **2014**, *4*, 4027-4033.
6  aX. Hong, D. Wang, Y. Li, *Chemical Communications* **2011**, *47*, 9909-9911; bL.-C. Cheng, J.-H. Huang, H. M. Chen, T.-C. Lai, K.-Y. Yang, R.-S. Liu, M. Hsiao, C.-H. Chen, L.-J. Her, D. P. Tsai, *Journal of Materials Chemistry* **2012**, *22*, 2244-2253; cY. Li, J. Ma, Z. Ma, *Electrochimica Acta* **2013**, *108*, 435-440; dV. W. K. Ng, R. Berti, F. Lesage, A. Kakkar, *Journal of Materials Chemistry B* **2013**, *1*, 9-25; eM. Li, J. W. Kang, R. R. Dasari, I. Barman, *Angewandte Chemie International Edition* **2014**, *53*, 14115-14119; fS. Z. Nergiz, N. Gandra, S. Tadepalli, S. Singamaneni, *ACS Applied Materials & Interfaces* **2014**, *6*, 16395-16402.
7  aA. P. Abbott, G. Capper, D. L. Davies, R. K. Rasheed, V. Tambyrajah, *Chemical Communications* **2003**, 70-71; bA. P. Abbott, D. Boothby, G. Capper, D. L. Davies, R. K. Rasheed, *Journal of the American Chemical Society* **2004**, *126*, 9142-9147.
8  Q. Zhang, K. De Oliveira Vigier, S. Royer, F. Jerome, *Chemical Society Reviews* **2012**, *41*, 7108-7146.
9  aE. L. Smith, A. P. Abbott, K. S. Ryder, *Chemical Reviews* **2014**, *114*, 11060-11082; bD. Carriazo, M. C. Serrano, M. C. Gutierrez, M. L. Ferrer, F. del Monte, *Chemical Society Reviews* **2012**, *41*, 4996-5014; cA. Carranza, J. A. Pojman, J. D. Mota-Morales, *RSC Advances* **2014**, *4*, 41584-41587; dR. J. Sanchez-Leija, J. A. Pojman, G. Luna-Barcenas, J. D. Mota-Morales, *Journal of Materials Chemistry B* **2014**, *2*, 7495-7501.
10  D. V. Wagle, H. Zhao, G. A. Baker, *Accounts of Chemical Research* **2014**, *47*, 2299-2308.
11  H.-G. Liao, Y.-X. Jiang, Z.-Y. Zhou, S.-P. Chen, S.-G. Sun, *Angewandte Chemie International Edition* **2008**, *47*, 9100-9103.
12  aM. Chirea, A. Freitas, B. S. Vasile, C. Ghitulica, C. M. Pereira, F. Silva, *Langmuir* **2011**, *27*, 3906-3913; bS. Stassi, V. Cauda, G. Canavese, D. Manfredi, C. F. Pirri, *European Journal of Inorganic Chemistry* **2012**, *2012*, 2669-2673; cL. Wei, Y.-J. Fan, H.-H. Wang, N. Tian, Z.-Y. Zhou, S.-G. Sun,

*Electrochimica Acta* **2012**, *76*, 468-474; dJ. A. Hammons, T. Muselle, J. Ustaroz, M. Tzedaki, M. Raes, A. Hubin, H. Terryn, *The Journal of Physical Chemistry C* **2013**, *117*, 14381-14389; eV. S. Raghuwanshi, M. Ochmann, F. Polzer, A. Hoell, K. Rademann, *Chemical Communications* **2014**, *50*, 8693-8696; fV. S. Raghuwanshi, M. Ochmann, A. Hoell, F. Polzer, K. Rademann, *Langmuir* **2014**, *30*, 6038-6046.

13  A. Pandey, S. Pandey, *The Journal of Physical Chemistry B* **2014**, *118*, 14652-14661.

14  H. You, F. Zhang, Z. Liu, J. Fang, *ACS Catalysis* **2014**, *4*, 2829-2835.

15  Y. Ma, Q. Kuang, Z. Jiang, Z. Xie, R. Huang, L. Zheng, *Angewandte Chemie International Edition* **2008**, *47*, 8901-8904.

16  H.-G. Liao, Y. Shao, C. Wang, Y. Lin, Y.-X. Jiang, S.-G. Sun, *Materials Letters* **2014**, *116*, 299-303.

17  R. He, Y.-C. Wang, X. Wang, Z. Wang, G. Liu, W. Zhou, L. Wen, Q. Li, X. Wang, X. Chen, J. Zeng, J. G. Hou, *Nature Communications* **2014**, *5*, 4327.

18  J. Xie, J. Y. Lee, D. I. C. Wang, *Chemistry of Materials* **2007**, *19*, 2823-2830.

19  A. Guerrero-Martínez, S. Barbosa, I. Pastoriza-Santos, L. M. Liz-Marzán, *Current Opinion in Colloid & Interface Science* **2011**, *16*, 118-127.

20  aT. S. Sreeprasad, A. K. Samal, T. Pradeep, *Langmuir* **2007**, *23*, 9463-9471; bX. Guo, W. Ye, R. Zhu, W. Wang, F. Xie, H. Sun, Q. Zhao, Y. Ding, J. Yang, *Nanoscale* **2014**, *6*, 11732-11737.

21  aJ.-Y. Dong, Y.-J. Hsu, D. S.-H. Wong, S.-Y. Lu, *The Journal of Physical Chemistry C* **2010**, *114*, 8867-8872; bA. Querejeta-Fernández, J. C. Hernández-Garrido, H. Yang, Y. Zhou, A. Varela, M. Parras, J. J. Calvino-Gámez, J. M. González-Calbet, P. F. Green, N. A. Kotov, *ACS Nano* **2012**, *6*, 3800-3812; cJ. Lu, X.-T. Li, E.-Q. Ma, L.-P. Mo, Z.-H. Zhang, *ChemCatChem* **2014**, *6*, 2854-2859; dH. Zheng, C.-D. Gu, X.-L. Wang, J.-P. Tu, *J Nanopart Res* **2014**, *16*, 1-9; eJ. Zhang, J. Chen, Q. Li, *Materials Research Bulletin* **2015**, *63*, 88-92; fC. Oumahi, J. Lombard, S. Casale, C. Calers, L. Delannoy, C. Louis, X. Carrier, *Catalysis Today* **2014**, *235*, 58-71; gC.-Y. Chen, K. Ozasa, F. Kitamura, K.-i. Katsumata, M. Maeda, K. Okada, N. Matsushita, *Electrochimica Acta* **2015**, *153*, 409-415; hY. Wang, Y. Xu, H. Ma, R. Xu, H. Liu, D. Li, Z. Tian, *Microporous and Mesoporous Materials* **2014**, *195*, 50-59; iM. O'Neill, V. S. Raghuwanshi, R. Wendt, M. Wollgarten, A. Hoell, K. Rademann, *Zeitschrift für Physikalische Chemie* **2014**, *229*, 221-234; jQ. Q. Xiong, J. P. Tu, X. Ge, X. L. Wang, C. D. Gu, *Journal of Power Sources* **2015**, *274*, 1-7.

22  A. Yadav, S. Pandey, *Journal of Chemical & Engineering Data* **2014**, *59*, 2221-2229.

23  aA. Kedia, P. S. Kumar, *RSC Advances* **2014**, *4*, 4782-4790; bS. E. Lohse, N. D. Burrows, L. Scarabelli, L. M. Liz-Marzán, C. J. Murphy, *Chemistry of Materials* **2014**, *26*, 34-43.

24  aT. H. Ha, H.-J. Koo, B. H. Chung, *The Journal of Physical Chemistry C* **2006**, *111*, 1123-1130; bW. Niu, S. Zheng, D. Wang, X. Liu, H. Li, S. Han, J. Chen, Z. Tang, G. Xu, *Journal of the American Chemical Society* **2008**, *131*, 697-703.

25  X. Xu, X. Zhang, H. Sun, Y. Yang, X. Dai, J. Gao, X. Li, P. Zhang, H.-H. Wang, N.-F. Yu, S.-G. Sun, *Angewandte Chemie International Edition* **2014**, *53*, 12522-12527.

26  [26]aJ. Xu, A. R. Wilson, A. R. Rathmell, J. Howe, M. Chi, B. J. Wiley, *ACS Nano* **2011**, *5*, 6119-6127; bZ. Li, Q. Niu, *ACS Sustainable Chemistry & Engineering* **2013**, *2*, 533-536.

27  W. Li, L. Kuai, Q. Qin, B. Geng, *Journal of Materials Chemistry A* **2013**, *1*, 7111-7117.

28  S.-G. Sun, A.-C. Chen, T.-S. Huang, J.-B. Li, Z.-W. Tian, *Journal of Electroanalytical Chemistry* **1992**, *340*, 213-226.

29  R. He, Y.-C. Wang, X. Wang, Z. Wang, G. Liu, W. Zhou, L. Wen, Q. Li, X. Wang, X. Chen, J. Zeng, J. G. Hou, *Nat Commun* **2014**, *5*.